Inorganic Chemistry

Article

pubs.acs.org/IC

Near-Infrared Quantum Cutting Platform in Thermally Stable Phosphate Phosphors for Solar Cells

Tzu-Chen Liu,[†] Gongguo Zhang,[‡] Xuebin Qiao,[§] Jing Wang,[‡] Hyo Jin Seo,[§] Din-Ping Tsai,[∇,⊥] and Ru-Shi Liu*[,†]

[†]Department of Chemistry, National Taiwan University, Taipei 106, Taiwan

[‡]School of Chemistry and Chemical Engineering, Sun Yat-sen University, Guangzhou, 510275, China

[§]Department of Physics, Pukyong National University, Busan 608-737, Korea

[∇]Department of Physics, National Taiwan University, Taipei 106, Taiwan

[⊥]Research Center for Applied Science, Academia Sinica, Taipei 115, Taiwan

ABSTRACT: This study investigated the photoluminescent properties of Tb^{3+}–Yb^{3+}-, Ce^{3+}–Tb^{3+}–Yb^{3+}-, and Eu^{2+}–Yb^{3+}-doped $KSrPO_4$. The samples were prepared by a solid-state reaction with various doping concentrations. Emission at near-infrared range was focused on the application of luminescent solar concentrator for solar cells. Quantum cutting (QC) energy transfer was confirmed by the lifetimes of the donor. Near-infrared QC involved emission of Yb^{3+} ions was achieved by excitation of Ce^{3+}, Tb^{3+}, and Eu^{2+} ions, where the energy transfer processes occurred from Ce^{3+} to Tb^{3+} to Yb^{3+}, Tb^{3+} to Yb^{3+}, and Eu^{2+} to Yb^{3+}, respectively. In addition, the concentration quenching effect of Yb^{3+} ions was avoided by low doping concentrations. The overall quantum efficiencies were calculated, and the maximum efficiency reaches 139%. The energy diagrams for divalent and trivalent rare-earth ions in $KSrPO_4$ host lattice were analyzed. Results of this study demonstrate that heat-stable phosphate phosphors are promising candidates for increasing the efficiency of silicon-based solar cells.

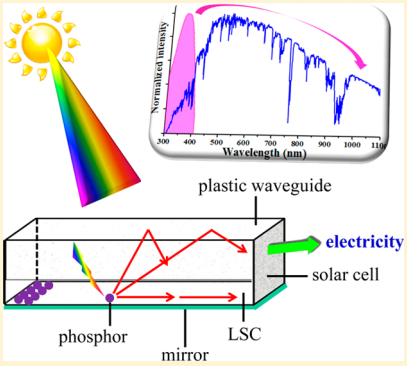

INTRODUCTION

The numerous energy levels of rare-earth (RE) ions make them available as energy converters. Phosphors doped with RE ions can convert incoming excitation sources into photons of different wavelength. Dexter proposed the concept of quantum cutting (QC) that yields multiple photons by cutting a high-energy photon to two lower-energy photons.[1] Theoretically, the quantum yield of this process can exceed 100%. The first experimental evidence for QC was demonstrated in YF_3:Pr^{3+}, where the two photons were emitted from the single Pr^{3+} ion.[2] Wegh et al. observed quantum cutting between two ions emitting visible photons in the Gd^{3+}–Eu^{3+} couple.[3]

QC has attracted increasing attention for its ability to improve solar cell efficiency. The terrestrial spectrum of the solar radiation on the surface of the earth (AM 1.5 G) has a large energy mismatch with the band gap of crystalline silicon (c-Si) wafer. Electron–hole pairs are generated when photons have energies much higher than the band gap of the semiconductor material. In addition, the excess energy of the electron–hole pairs is dissipated as heat. The thermalization process largely explains the efficiency loss. Solar cell efficiency can be increased if the high-energy visible photons are converted to near-infrared (NIR) photons.[4] Close examination of the Dieke diagram[5] reveals that the energy of the Yb^{3+} $^2F_{5/2}$ → $^2F_{7/2}$ transition is located at ~10 000 cm^{-1}, which is just above the band gap of c-Si. Several RE–Yb^{3+} donor–acceptor couples have been developed to convert one visible photon shorter than 500 nm to two NIR photons such as Tb^{3+}–Yb^{3+}, Tm^{3+}–Yb^{3+}, Pr^{3+}–Yb^{3+}, Er^{3+}–Yb^{3+}, Nd^{3+}–Yb^{3+}, and Ho^{3+}–Yb^{3+}.[6−10] However, the photoluminescence excitation strengths of donors from the forbidden 4f → 4f transitions are generally low, and the absorption bandwidths are always narrow. Two alternative approaches have been proposed to solve this problem: (1) adding a sensitizer to transfer the excited energy to the donor with 4f → 4f transitions,[11] and (2) using a broad band donor such as Eu^{2+} and Ce^{3+} ions.[12,13]

Although many approaches have been demonstrated to elucidate the NIR quantum cutting effect, their luminescent properties have not been compared. This study focuses on the three combinations of RE–Yb^{3+} ions: (1) Tb^{3+}–Yb^{3+}, where the Tb^{3+} $^5D_4$ → $^7F_6$ transition is located at around twice the energy of the Yb^{3+} $^2F_{5/2}$ → $^2F_{7/2}$ transition, (2) Ce^{3+}–Tb^{3+}–Yb^{3+}, where Ce^{3+} ion transfers its 5d → 4f energy to the $^5D_4$ level of Tb^{3+} ion, (3) Eu^{2+}–Yb^{3+}, where Eu^{2+} ion functions as an energy transfer donor. $KSrPO_4$ is chosen as a phosphate host lattice, which has a tridymite structure (β-SiO_2).[14] Its structure involves the PO_4^{3-} tetrahedron that surrounds the K^+ and Sr^{2+} cations in 10-fold and 9-fold coordination, respectively; in addition, it exhibits satisfactory chemical and thermal stabilities.[15,16] In a solar cell device, sunlight energy is not collected directly by the semiconductor solar cell. As a

Received: November 22, 2012
Published: June 7, 2013

transparent polymer plastic sheet in which luminescent species are dispersed, a luminescent solar concentrator absorbs the incident sunlight first and then guides it to the solar cell by total internal reflection. Therefore, thermal stability is a priority concern, because of the direct irradiation of sunlight.[17]

This study examines the energy transfer mechanism and the effect of the concentration of activators. NIR signals are detected in the three systems. Based on the results of this study, we conclude that the Eu^{2+}–Yb^{3+} system is a better choice when using QC for solar cells.

EXPERIMENTAL SECTION

Synthesis. The powder samples of $KSrPO_4$ phosphates were prepared by a conventional solid-state reaction. The starting materials KH_2PO_4 99.9%, $SrCO_3$ 99.9%, Eu_2O_3 99.9%, CeO_2 99.9%, Tb_4O_7 99.9%, and Yb_2O_3 99.9% were weighed in stoichiometric amounts and subsequently mixed and ground together by grinding in an agate mortar. The powder mixtures were synthesized by sintering at 1300 °C for 3 h in a reductive atmosphere (5% H_2/95% N_2). The as-synthesized samples were then cooled to room temperature inside a tube furnace under 5% H_2/95% N_2 flow. Finally, the samples were ground into powder for subsequent analysis.

Characterization. The composition and phase purity of the samples were studied by X-ray diffraction (XRD), using a PANalytical XPert'Pert PRO system with Cu Kα radiation (λ = 1.5418 Å) operated at 45 kV and 40 mA. The data were collected over a 2θ range of 20°–60° at intervals of 0.02° with a counting time of 30 s per step. The photoluminescence excitation (PLE) and emission (PL) spectra were measured at room temperature by a combined time-resolved and steady-state fluorescence spectrometer (Model FSP920, Edinburgh Instruments) equipped with thermo-electric cooled red sensitive photomultiplier tube (PMT) and a near-infrared photomultiplier tube (NIR-PMT) in a liquid-nitrogen-cooled housing (Model R5509-72, Hamamatsu Photonics K.K).

RESULTS AND DISCUSSION

Tb^{3+}–Yb^{3+} and Ce^{3+}–Tb^{3+}–Yb^{3+} Systems. Figure 1a shows the XRD patterns of KSP:RE samples (where KSP = $KSrPO_4$ and RE = Ce^{3+}, Tb^{3+}, Ce^{3+}–Tb^{3+}, Ce^{3+}–Tb^{3+}–Yb^{3+}). All experimental XRD patterns of the samples were identified by comparison with the reference JCPDS Database No. 33-1045. $KSrPO_4$ has an orthorhombic structure with space group *Pnma* and lattice constants $a \neq b \neq c$, $\alpha = \beta = \gamma = 90°$, as shown in Figure 1b. This comparison reveals that the expected compounds were synthesized successfully. Asterisks observed at 2θ = 29.7° and 33.5° in Figure 1a indicate the presence of a small unknown impurity phase when the concentrations of the doped activators are high. Notably, a small quantity of impurity phases negligibly affects the energy transfer. A previous study[18] found similar impurity phases, and the impurity phases were observed when the substitution of RE to Sr ions was >0.02. The presence of small impurities phases could be due to the size mismatch of Sr ions to RE ions: Sr^{2+} (9 CN, 1.31 Å), Ce^{3+} (9 CN, 1.20 Å), Tb^{3+} (9 CN, 1.10 Å), Yb^{3+} (9 CN, 1.01 Å), and Eu^{2+} (9 CN, 1.30 Å).[19] [CN denotes coordination number.]

Figure 2 plots the photoluminescence excitation (PLE) and emission (PL) spectra of KSP:RE, where RE = Ce^{3+}, Tb^{3+}, Ce^{3+}–Tb^{3+}. For KSP doped with 0.005 Ce^{3+} (Figure 2a), this figure reveals a broad-band emission in the ultraviolet (UV) region, which can be deconvoluted into two Gaussian components with peaks at 330 and 355 nm. The spin–orbital splitting of the 4f ground state of Ce^{3+} ion is 2000 cm^{-1} apart. For KSP:0.02 Tb^{3+} (Figure 2b), several characteristic sharp emissions are due to the $^5D_{4/3} \rightarrow {}^7F_J$ (J = 6, 5, 4, and 3) transitions of Tb^{3+} ion where 412, 433, 455, and 471 nm belong

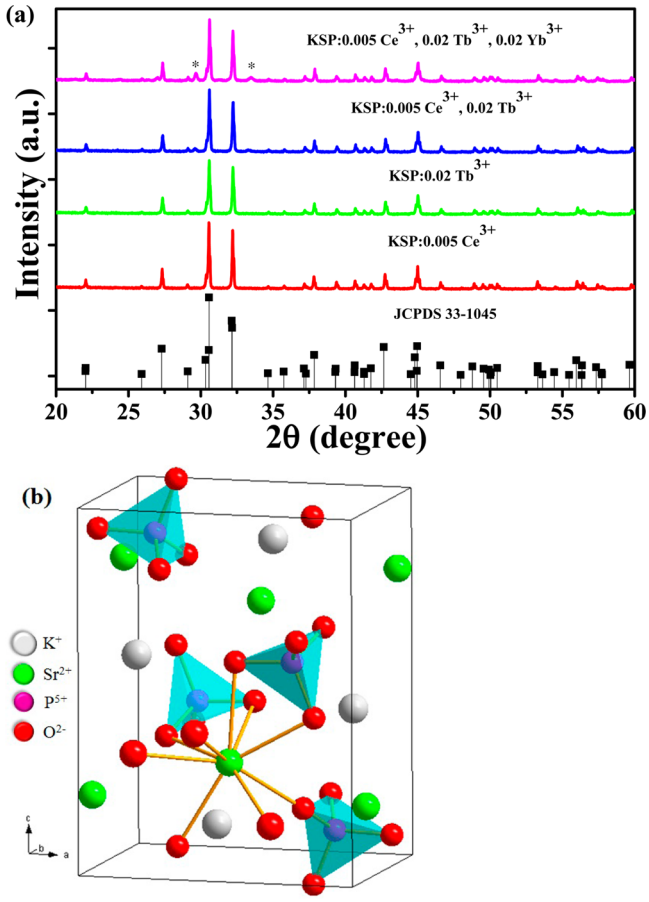

Figure 1. (a) Powder XRD patterns of $KSrPO_4$:RE, where RE = 0.005 Ce^{3+}; 0.02 Tb^{3+}; 0.005 Ce^{3+} and 0.02 Tb^{3+}; and 0.005 Ce^{3+}, 0.02 Tb^{3+}, and 0.02 Yb^{3+}. (b) Unit cell of $KSrPO_4$.

to $^5D_3 \rightarrow {}^7F_J$ transitions and 484, 543, 584, and 620 nm belong to $^5D_4 \rightarrow {}^7F_J$ transitions. Monitoring the dominating green emission peak at 541 nm, a few sharp peaks due to the forbidden 4f → 4f transitions of Tb^{3+} ions are observed in the wavelength range of 280–500 nm. The emission and excitation intensities of Tb^{3+} ions are magnified by a factor of 5. The PL of KSP:0.005 Ce^{3+} and the PLE of KSP:0.02 Tb^{3+} clearly indicate that an extended overlap exists, revealing that effective sensitizing is expected in the Ce^{3+}–Tb^{3+} pairs. Figure 2c shows the effect of codoping Ce^{3+} ions. Upon excitation of Ce^{3+} ions at 310 nm, the intensity of Tb^{3+} ions at 541 nm is 33 times higher when it is excited by $^7F_6 \rightarrow {}^5D_4$ transition at 484 nm. This finding suggests that an effective energy transfer (ET) from Ce^{3+} ions to Tb^{3+} ions occurs. Figure 2d shows the PL spectra of KSP:Ce^{3+}–Tb^{3+}. According to this figure, the emission intensity of Tb^{3+} ions increases at the expense of Ce^{3+} ions. The lifetime of Ce^{3+} ions is 26.7 ns for KSP:0.002 Ce^{3+}, and then gradually declines to 22.2 ns as the concentration of Tb^{3+} ions increases from 0 to 2%. This observation further demonstrates the presence of energy transfer in the KSP:Ce^{3+}–Tb^{3+} system. The ET efficiency (η_{ET}) can be calculated using the following equation:[20]

$$\eta_{ET} = 1 - \frac{\tau_0}{\tau}$$

where τ_0 and τ are the lifetimes of Ce^{3+} ions in the absence and presence of Tb^{3+} ions, respectively. Notably, the η_{ET} value reaches 17% when the maximum concentration of Tb^{3+} ions is

dx.doi.org/10.1021/ic302561r | Inorg. Chem. 2013, 52, 7352–7357

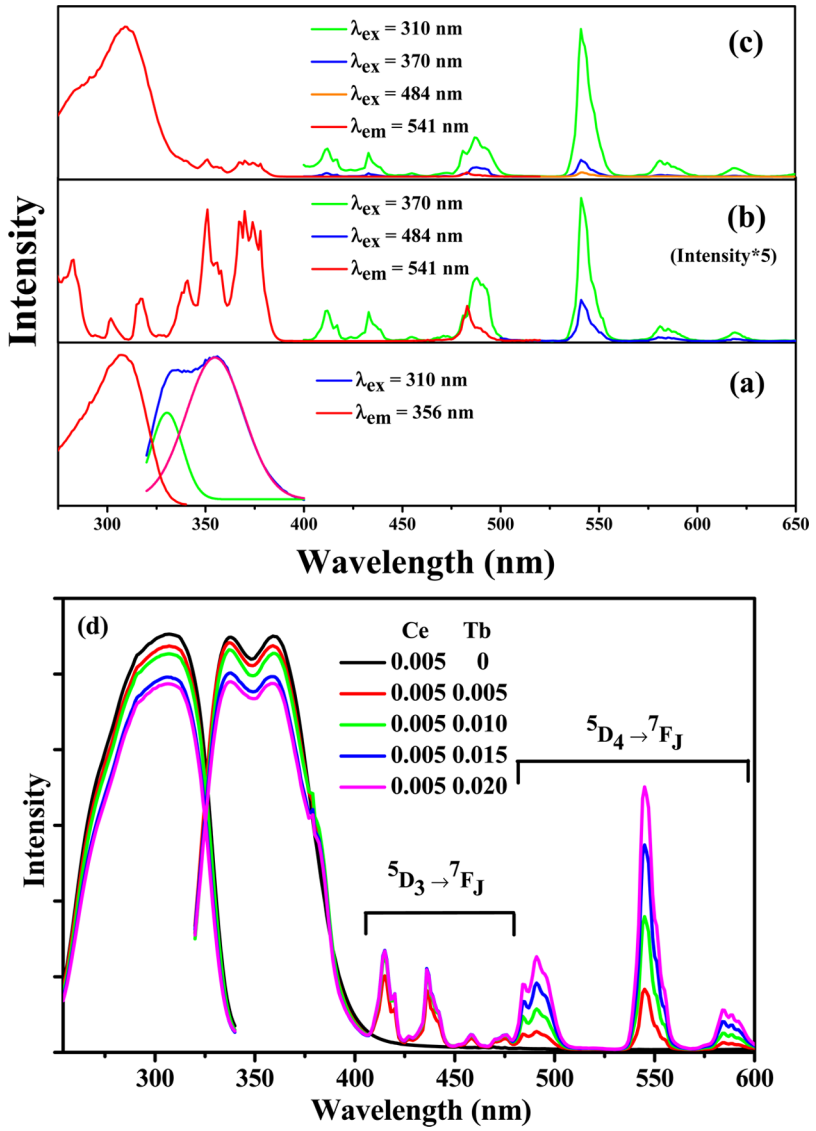

Figure 2. Excitation and emission spectra of $KSrPO_4$:RE, where RE = (a) 0.005 Ce^{3+}, (b) 0.02 Tb^{3+}, (c) 0.005 Ce^{3+} and 0.02 Tb^{3+}, and (d) 0.005 Ce^{3+}, x Tb^{3+} (x = 0, 0.005, 0.01, 0.015, 0.02).

2%. The concentration of Tb^{3+} does not increase further, because the increase in the amount of activators leads to impurity phases. Interestingly, the intensities of transitions from the $^5D_3$ level do not increase more significantly than those of the transitions from the $^5D_4$ level. This finding implies the presence of a nonradiative de-excitation pathway, such as cross relaxation between $^5D_3 \rightarrow {}^5D_4$.[21]

In the Tb^{3+}–Yb^{3+} and Ce^{3+}–Tb^{3+}–Yb^{3+} systems, the ET and QC processes can be expressed as follows: when the Ce^{3+} ions are excited by 310 nm photons, electrons can either relax to the $4f^1$ ground states by emitting 330 and 355 nm light or transfer the energy to the $^5D_3$ level of Tb^{3+} ions. A nonradiative de-excitation pathway then relaxes electrons from $^5D_3$ to $^5D_4$ level. QC subsequently occurs from the $^5D_4$ level of a Tb^{3+} ion to two different Yb^{3+} ions. Finally, emission near 1000 nm from the $^2F_{5/2} \rightarrow {}^2F_{7/2}$ transition can be detected. In the Tb^{3+}–Yb^{3+} system, the QC process is similar, except that Tb^{3+} ions can be excited to different excited states by excitation of 370 or 484 nm photons.

To increase the efficiency of solar cells, this study examines the effect of the sensitizer by the intensity of the NIR signal in Figure 3. This figure compares the NIR emission spectra of KSP doped with Tb^{3+}–Yb^{3+} and Ce^{3+}–Tb^{3+}–Yb^{3+} systems,

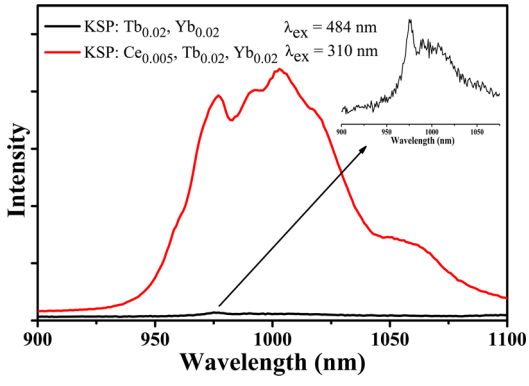

Figure 3. Emission spectra of $KSrPO_4$:RE at the near-infrared (NIR) region, where RE = 0.005 Ce^{3+}, 0.02 Tb^{3+}, 0.02 Yb^{3+} and 0.02 Tb^{3+}, 0.02 Yb^{3+}. The intensity of $KSrPO_4$:0.02 Tb^{3+}, 0.02 Yb^{3+} is magnified for clarity.

dx.doi.org/10.1021/ic302561r | Inorg. Chem. 2013, 52, 7352–7357

which are excited by 484 and 310 nm photons, respectively. It is obvious that, when a small amount of the sensitizer is added, the NIR signal increases dramatically. The signal of Tb^{3+}–Yb^{3+} pairs is magnified in the inset. The integration area is 20 times larger with the presence of Ce^{3+} ions. Our results thus demonstrate that a triactivator Ce^{3+}–Tb^{3+}–Yb^{3+} system can be a platform for NIR QC phosphor for c-Si solar cells.[22]

Eu^{2+}–Yb^{3+} system. This section describes the synthesis of the QC Eu^{2+}–Yb^{3+} system with a donor having a broad band excitation to verify its feasibility. The concentration of the activator is kept at 0.5% for Eu^{2+}, and that of Yb^{3+} concentration is changed from 0 to 1%. Theoretically, the QC efficiency rises with an increasing number of Yb^{3+} ions. However, concentration quenching of Yb^{3+} becomes significant at a high concentration, explaining why the NIR quantum efficiency is reduced. The XRD patterns for each composition are confirmed to be single phases (data not shown). Figure 4a

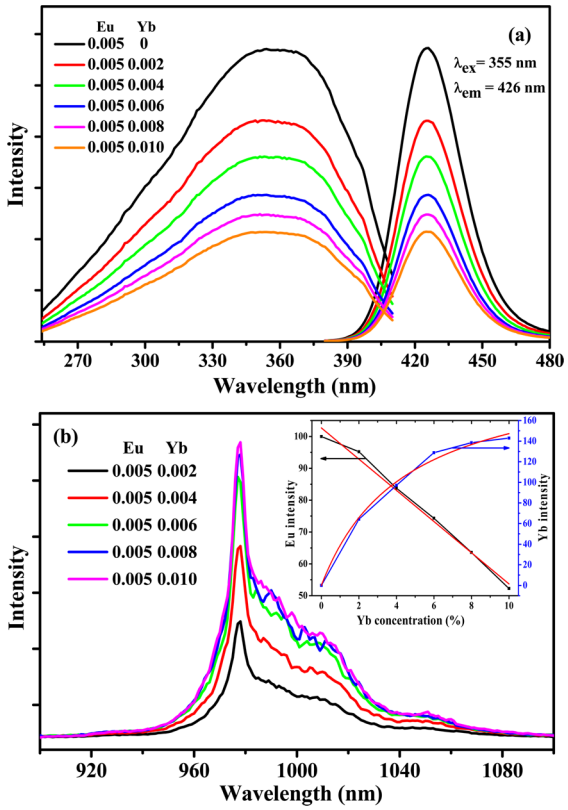

Figure 4. (a) Excitation and emission spectra of $KSrPO_4$:RE, where RE = 0.005 Eu^{2+}, x Yb^{3+} (x = 0, 0.002, 0.004, 0.006, 0.008, 0.010). (b) Emission spectra of $KSrPO_4$:RE at the NIR region, where RE = 0.005 Eu^{2+}, x Yb^{3+} (x = 0.002, 0.004, 0.006, 0.008, 0.010); the inset shows the linear fitting of the degree in which Eu^{2+} decreases and Yb^{3+} increases.

plots the PL and PLE spectra of KSP:RE, where RE = 0.005 Eu^{2+}, x Yb^{3+} (x = 0–1%). This figure reveals that the emission intensity of Eu^{2+} ions decreases sharply with increasing number of Yb^{3+} ions. The excitation band of Eu^{2+} ions has its highest intensity at 355 nm, which is much more red-shifted than that of Ce^{3+} ions. Figure 4b shows the NIR emission spectra of the samples with different Yb^{3+} concentration. Notably, the degrees of the emission decreasing of Eu^{2+} ions and the emission increasing of Yb^{3+} ions differ from each other. According to the inset of Figure 4b, Eu^{2+} decreases linearly, while Yb^{3+} ions can be fitted to be a nonlinear curve. This phenomenon further confirms that the concentration of Yb^{3+} ions cannot be too high.

Figure 5 plots the lifetimes of Eu^{2+} ions of KSP:RE, where RE = 0.005 Eu^{2+}, x Yb^{3+} (x = 0, 0.002, 0.004, 0.006, 0.008, and

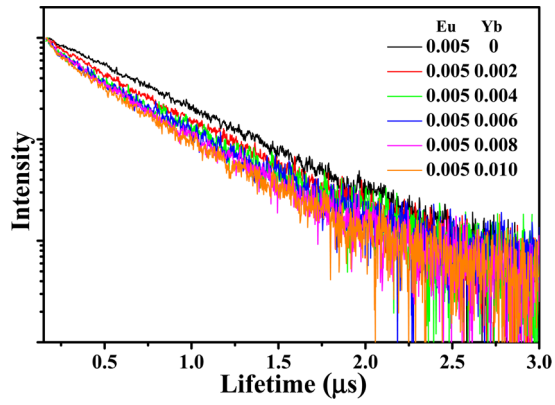

Figure 5. Decay curves of $KSrPO_4$:RE excited by 355 nm, monitored at 426 nm, RE = 0.005 Eu^{2+}, x Yb^{3+} (x = 0, 0.002, 0.004, 0.006, 0.008, 0.010).

0.01) monitored at 426 nm. The second-order decay curves are fitted by:[23]

$$I = A_1 \exp\left(-\frac{t}{\tau_1}\right) + A_2 \exp\left(-\frac{t}{\tau_2}\right) + C$$

where I is the luminescence intensity; A_1, A_2, and C are constants; t is the time; and τ_1 and τ_2 are the rapid and slow lifetimes, respectively. The average lifetime (τ^*) can be calculated using the following formula:

$$\tau^* = \frac{A_1\tau_1^2 + A_2\tau_2^2}{A_1\tau_1 + A_2\tau_2}$$

The calculated Eu^{2+} lifetimes are 0.38, 0.29, 0.24, 0.22, 0.21, and 0.19 μs for KSP:RE, where RE = 0.005 Eu^{2+}, $x$$Yb^{3+}$ (x = 0, 0.002, 0.004, 0.006, 0.008, and 0.01).

In the Eu^{2+}–Yb^{3+} pairs, the energy transfer efficiency (η_{ETE}) is defined as the ratio of Eu^{2+} ions that are depopulated by ET to Yb^{3+} ions over the total number of the excited Eu^{2+} ions. Assume that all excited Yb^{3+} ions decay radiatively, the η_{ETE} can be determined by the following equation, in which the integrated intensity of the decay curve of Eu^{2+} singly doped sample is divided by that of the Eu^{2+}–Yb^{3+} pairs:[6]

$$\eta_{ETE} = 1 - \frac{\int I_{x\%Yb}\,dt}{\int I_{0\%Yb}\,dt}$$

where I is the intensity and x%Yb is the concentration of Yb^{3+} ions.

The total QC quantum yield (η_{QE}) is the ratio of photnons emitted to the number of photons that are absorbed, which is defined as:[6]

$$\eta_{QE} = \eta_{Eu}(1 - \eta_{ETE}) + 2\eta_{ETE}$$

where nonradiative energy loss by defects and impurities is ignored, so that η_{Eu} is set to a value of 1.

Table 1 summarizes the NIR QE and the decay lifetimes of Eu^{2+} ions versus different Yb^{3+} doping concentrations.

dx.doi.org/10.1021/ic302561r | Inorg. Chem. 2013, 52, 7352–7357

Table 1. Relationship of Eu^{2+} Lifetime and QC Quantum Yield with Different Concentrations of Yb^{3+} Ions

Yb^{3+} concentration (%)	Eu^{2+} lifetime (μs)	η_{QE} (%)
0	0.38	100
0.2	0.29	118
0.4	0.24	129
0.6	0.22	131
0.8	0.21	134
1.0	0.19	139

According to Figure 4b, the concentration quenching of Yb^{3+} ions is avoided, so the value of η_{QE} reaches its maximum value of 139% when the doping concentration of Yb^{3+} ions is 1%. This finding suggests that the NIR QC for the KSP:Eu^{2+}–Yb^{3+} system is highly efficient.

Energy-Level Schemes of $KSrPO_4$:RE. From the data of doping a $KSrPO_4$ host with several different RE ions, the parameters of the host lattice affecting the luminescent properties can be obtained. According to the formula developed by Dorenbos, the df emission of RE ions can be written as:[24]

$$E_{em}(n, Q, A) = E_{free}(n, Q) - D(Q, A) - \Delta S(Q, A)$$

where E_{em} is the emission wavelength, E_{free} is the energy of gas (free) RE ions, n is the number of the electrons at 4f orbitals, Q is the valency, and A is the host lattice. In addition, $D(Q,A)$ is called a red-shift, which is determined by the centroid shift and crystal field splitting. Moreover, $\Delta S(Q,A)$ refers to the Stokes shift. Therefore, two formulas can be written as follows:

$$E_{em}(1, +3, KSrPO_4) = E_{free}(1, +3) - D(+3, KSrPO_4) - \Delta S(+3, KSrPO_4) \quad (1)$$

$$E_{em}(6, +2, KSrPO_4) = E_{free}(6, +2) - D(+2, KSrPO_4) - \Delta S(+2, KSrPO_4) \quad (2)$$

where formulas 1 and 2 are for Ce^{3+} and Eu^{2+} ions, respectively. The values of D and ΔS are dependent only on the host lattice. The energies of gaseous Ce^{3+} and Eu^{2+} ions are 49 300 and 34 000 cm^{-1}, respectively.[25] From the luminescent data, $D(+2, KSrPO_4)$ and $\Delta S(+2,KSrPO_4)$ are 5800 and 4700 cm^{-1}; $D(+3, KSrPO_4)$ and $\Delta S(+3,KSrPO_4)$ are 16700 and 2300 cm^{-1}. Another formula developed by Dorenbos reveals that the location of df transitions of other RE^{3+} ions could be evaluated by the energy difference between Ce^{3+} ions ($\Delta E^{RE,Ce}$).[26] The excitation peaks of Pr^{3+} and Tb^{3+} ions are confirmed and located at 220 and 215 nm, which are 13 900 and 12 400 cm^{-1} higher than that of Ce^{3+} ions, respectively. The formula is also valid for divalent RE ions. A previous study found an emission peak of Sm^{2+} ions from the 4f → 5d transition at 715 nm,[27] which is 9500 cm^{-1} lower than that of Eu^{2+} ions. The resulting energy level and QC scheme for $KSrPO_4$ lattice are constructed in Figure 6a. Figure 6b compares the excitation bands of Ce^{3+} and Eu^{2+} ions with those of AM 1.5 G spectrum. It is obvious that due to the high energy of photons required to excite Ce^{3+} ions, the excitation band only overlaps with AM 1.5 G spectrum narrowly. The excitation spectrum of Eu^{2+} ions ranges from 300 nm to 420 nm, which shows a much better overlap than that of Ce^{3+} ions. This finding suggests that Eu^{2+} ions is a better donor in the quantum cutting process.

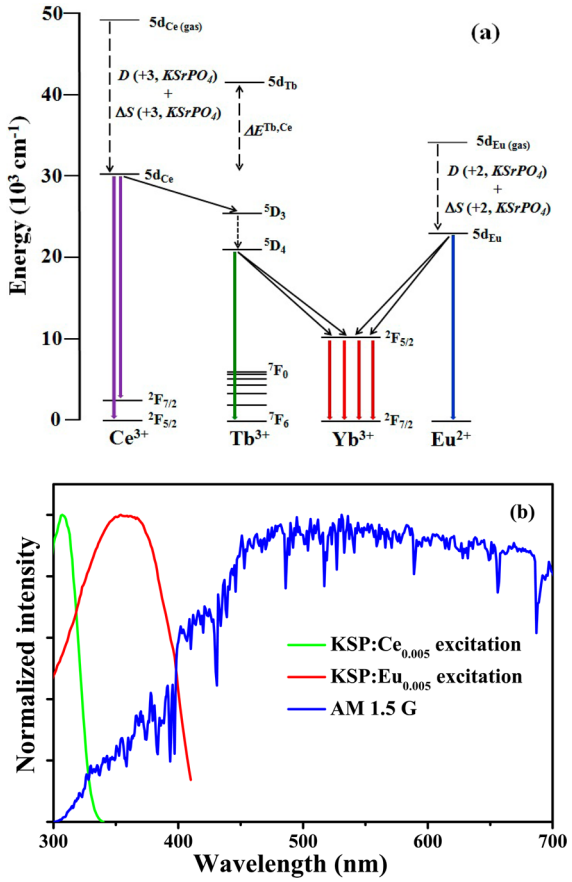

Figure 6. (a) Schematic energy level diagrams for NIR QC and energy transfer in $KSrPO_4$ lattice doped with a triactivator Ce^{3+}–Tb^{3+}–Yb^{3+} system and a diactivator Eu^{2+}–Yb^{3+} system. (b) Overlapped spectra of AM 1.5 G with the excitation of Ce^{3+} and Eu^{2+} ions doped in $KSrPO_4$ lattice with intensity normalized.

CONCLUSION

This study investigates the behaviors of quantum cutting by doping a triactivator Ce^{3+}–Tb^{3+}–Yb^{3+} system and two diactivator systems of Tb^{3+}–Yb^{3+} and Eu^{2+}–Yb^{3+} in $KSrPO_4$ lattice. Based on the photoluminescence spectra and lifetimes, we conclude that both systems undergo QC process and have NIR signals detected. The calculated quantum efficiency reaches its maximum value of 139% when the doping concentration of Yb^{3+} ions is 1%. The measured quantum yield is closer to the real value, since the concentration quenching of Yb^{3+} is avoided. The development of NIR QC phosphors, which correlates well with the spectral response of silicon-based solar cells, provides an alternative means of increasing the efficiency of luminescent solar concentrators. Based on an energy diagram that plots the effect of host lattice to the 5d levels of trivalent and divalent rare-earth ions, we believe that the lower energy of Eu^{2+} ions makes it better as a donor in the QC process.

AUTHOR INFORMATION

Corresponding Author

*E-mail: rsliu@ntu.edu.tw.

Notes

The authors declare no competing financial interest.

dx.doi.org/10.1021/ic302561r | Inorg. Chem. 2013, 52, 7352–7357

■ ACKNOWLEDGMENTS

The authors would like to thank the National Science Council of Taiwan (Contract No. NSC 101-2113-M-002-014-MY3) for financially supporting this research.

■ REFERENCES

(1) Dexter, D. L. *Phys. Rev.* **1957**, *108*, 630.
(2) Sommerdijk, J. L.; Bril, A.; de Jager, A. W. *J. Lumin.* **1974**, *8*, 341.
(3) Wegh, R. T.; Donker, H.; Oskam, K. D.; Meijerink, A. *Science* **1999**, *283*, 663.
(4) (a) Trupke, T.; Green, M. A.; Würfel, P. *J. Appl. Phys.* **2002**, *92*, 1668. (b) Huang, X.; Han, S.; Huang, W.; Liu, X. *Chem. Soc. Rev.* **2013**, *42*, 173.
(5) Dieke, G. H. *Spectra and Energy Levels of Rare Earth Ions in Crystals*: Interscience: New York, 1968.
(6) Vergeer, P.; Vlugt, T. J. H.; Kox, M. H. F.; den Hertog, M. I.; van der Eerden, J.; Meijerink, A. *Phys. Rev. B* **2005**, *71*, 014119.
(7) Zhang, Q. Y.; Yang, G. F.; Jiang, Z. H. *Appl. Phys. Lett.* **2007**, *91*, 051903.
(8) Meijerink, J. M.; Aarts, L.; van der Ende, B. M.; Vlugt, T. J. H.; Meijerink, A. *Phys. Rev. B* **2010**, *81*, 035107.
(9) Eilers, J. J.; Biner, D.; van Wijngaarden, J. T.; Krämer, K.; Güdel, H.-U.; Meijerink, A. *Appl. Phys. Lett.* **2010**, *96*, 151106.
(10) Deng, K.; Gong, T.; Hu, L.; Wei, X.; Chen, Y.; Yin, M. *Opt. Exp.* **2011**, *19*, 1749.
(11) Zhang, Q.; Wang, J.; Zhang, G.; Su, Q. *J. Mater. Chem.* **2009**, *19*, 7088.
(12) Zhou, J.; Zhuang, Y.; Ye, S.; Teng, Y.; Lin, G.; Zhu, B.; Xie, J.; Qiu, J. *Appl. Phys. Lett.* **2009**, *95*, 141101.
(13) Ueda, J.; Tanabe, S. *J. Appl. Phys.* **2009**, *106*, 043101.
(14) Elammari, L.; El Koumiri, M.; Zschokke-Granacher, I.; Elouadi, B. *Ferroelectrics* **1994**, *158*, 19.
(15) Tang, Y. S.; Hu, S. F.; Lin, C. C.; Bagkar, N. C.; Liu, R. S. *Appl. Phys. Lett.* **2007**, *90*, 151108.
(16) Lin, C. C.; Xiao, Z. R.; Guo, G. Y.; Chan, T. S.; Liu, R. S. *J. Am. Chem. Soc.* **2010**, *132*, 3020.
(17) van Sark, W. G. J. H. M.; Barnham, K. W. J.; Sloof, L. H.; Chatten, A. J.; Büchtemann, A.; Meyer, A.; McCormack, S. J.; Koole, R.; Farrell, D. J.; Bose, R.; Bende, E. E.; Burgers, A. R.; Budel, T.; Quilitz, J.; Kennedy, M.; Meyer, T.; Donega, C. de M.; Meijeriink, A.; Vanmaekelbergh, D. *Opt. Express* **2008**, *16*, 21773.
(18) Lin, C. C.; Liu, R. S.; Tang, Y. S.; Hu, S. F. *J. Electrochem. Soc.* **2008**, *155*, J248.
(19) Shannon, R. D. *Acta Crystallogr., Sect. A: Cryst. Phys., Diffr., Theor. Gen. Crystallogr.* **1976**, *32*, 751.
(20) Paulose, P. I.; Jose, G.; Thomas, V.; Unnikrishnan, N. V.; Warrier, M. K. R. *J. Phys. Chem. Solids* **2003**, *64*, 841.
(21) Ricci, P. C.; Carbonaro, C. M.; Corpino, R.; Cannas, C.; Salis, M. *J. Phys. Chem. C* **2011**, *115*, 16630.
(22) Huang, X. Y.; Yu, D. C.; Zhang, Q. Y. *J. Appl. Phys.* **2009**, *106*, 113521.
(23) Huang, C. H.; Chen, T. M. *J. Phys. Chem. C* **2011**, *115*, 2349.
(24) van der Kolk, E.; Dorenbos, P.; Vink, A. P.; Perego, R. C.; van Eijk, C. W. E. *Phys. Rev. B* **2001**, *64*, 195129.
(25) Dorenbos, P. *J. Lumin.* **2003**, *104*, 239.
(26) Dorenbos, P. *J. Lumin.* **2000**, *91*, 155.
(27) Huang, Y.; Kai, W.; Cao, Y.; Jang, K.; Lee, H. S.; Kim, I.; Cho, E. *J. Appl. Phys.* **2008**, *103*, 053501.